Materials Horizons

ROYAL SOCIETY OF CHEMISTRY

COMMUNICATION

View Article Online
View Journal | View Issue



Cite this: *Mater. Horiz.*, 2023, **10**, 257

Received 16th August 2022,
Accepted 15th November 2022

DOI: 10.1039/d2mh01016j

rsc.li/materials-horizons

# Passive climate regulation with transpiring wood for buildings with increased energy efficiency†

Yong Ding, [ab] Christopher H. Dreimol, [ab] Robert Zboray, [c] Kunkun Tu, [ab] Sandro Stucki, [ab] Tobias Keplinger, [ab] Guido Panzarasa [ab] and Ingo Burgert *[ab]

**Buildings are significant end-users of global energy. About 20% of the energy consumption worldwide is used for maintaining a comfortable indoor climate. Therefore, passive systems for indoor temperature and humidity regulation that can respond to environmental changes are very promising to reduce buildings' energy consumption. We developed a process to improve the responsiveness of wood to humidity changes by laser-drilling microscopic holes and incorporating a hygroscopic salt (calcium chloride). The resulting "transpiring wood" displays superior water adsorption capacity and high moisture exchange rate, allowing regulation of humidity and temperature by the exchange of moisture with the surrounding air. We proved that the hygrothermal performance of transpiring wood can be used to regulate indoor climate, with associated energy savings, for various climate types, thus favoring its application in the building sector. The reduction of temperature fluctuations, thanks to the buffering of temperature peaks, can lead to an indirect energy saving of about 10% for cooling and between 4–27% for heating depending on the climate. Furthermore, our transpiring wood meets different sustainability criteria, from raw materials to the fabrication process, resulting in a product with a low overall environmental impact and that is easy to recycle.**

### New concepts

About 20% of energy consumption around the world is used for maintaining a comfortable indoor climate. Developing materials that are able to respond to diurnal humidity/temperature changes would be highly relevant for energy-saving buildings, *e.g.* for passive indoor thermal and/or humidity regulation purposes. Herein, we successfully develop "transpiring wood" that shows superior humidity and temperature regulation performance by the exchange of moisture with the environment. Our transpiring wood can help self-regulating indoor humidity levels for living comfort, resulting in energy savings for different climate types. By decreasing the indoor temperature fluctuations, we calculated an indirect energy saving in the order of 10% for cooling, and up to 27% for heating. These findings have great practical relevance in terms of energy-saving and favor the broad application of transpiring wood in the building sector. Furthermore, our transpiring wood meets sustainability criteria due to the use of renewable resources and a green fabrication process.

## Introduction

Buildings account for more than 35% of the entire energy consumption, making them an important factor in countries' energy-saving plans worldwide. About 50% of the total energy consumed by buildings is used to maintain a comfortable indoor climate, fundamental for the occupants' well-being and health.[1] Reducing the energy necessary for building operations, while maintaining or even improving living comfort, is a pressing challenge for sustainable development, especially in view of the ongoing climate change (Fig. S1, ESI†).[2–4]

Functional materials able to respond to environmental stimuli such as seasonal and diurnal weather changes can be used to design passive systems for humidity and/or thermal regulation operating with no or very low energy input, which is very promising for implementation in energy-saving buildings. Passive humidity regulation systems rely on desiccating materials that are able to adsorb and release moisture such as zeolites, silica gels, metal–organic frameworks (MOFs), and hydrogels.[5–7] For example UiO-67-4Me-$NH_2$, a moderately hydrophilic MOF which displays a high water sorption capacity in the comfortable range of indoor relative humidity.[8] Passive thermal regulation systems can be obtained using materials that are able to store thermal energy or reduce the thermal exchange with the environment, such as phase-change materials or porous insulators, respectively.[9,10] Previous work by Wei *et al.*[11] reported 3D-printed polymeric phase change material (PCM) composites as effective thermal buffers across the melting temperature range of the PCM (45–65 °C), allowing to mitigate temperature fluctuations

[a] *Wood Materials Science, Institute for Building Materials, ETH Zürich, 8093, Zürich, Switzerland. E-mail: iburgert@ethz.ch*
[b] *WoodTec Group, Cellulose & Wood Materials, Empa, 8600 Dübendorf, Switzerland*
[c] *Center for X-ray Analytics, Empa, 8600 Dübendorf, Switzerland*

† Electronic supplementary information (ESI) available. See DOI: https://doi.org/10.1039/d2mh01016j

(10% lower while heating, 40% higher while cooling) compared to control setups. It is noteworthy that only a few reports exist for passive systems allowing contemporary management of humidity and temperature. This is mainly due to the limitations of state-of-art materials and composites in terms of large-scale fabrication, recycling, and installation.

Wood is widely available, lightweight, equipped with very good mechanical performance, therefore an excellent building material since ancient times.[12] Furthermore, it is a renewable and $CO_2$-storing natural resource. Wood is naturally hygroscopic because of its highly porous structure and a large number of accessible hydroxyl groups. However, for practical applications wood hygroscopicity is usually considered as a serious flaw. The reversible uptake and release of moisture results in dimensional instability due to swelling and shrinking. Moreover, with high moisture content wood can become prone to fungal degradation. Therefore, countless technological efforts have been devoted to reducing wood's moisture uptake.[13]

In the present work, we demonstrate that this intrinsic characteristic of wood can be turned from a problem into a powerful asset for the design of indoor climate-regulating, energy-saving building materials. Thanks to a combination of laser-drilled pores and impregnation with calcium chloride $CaCl_2$ (a state-of-art desiccating agent), we dramatically increased the responsiveness of wood to environmental humidity changes. Thanks to its improved humidity exchange properties, our "transpiring wood" allows the efficient passive management of indoor climate (humidity and temperature) while maintaining a mechanical strength sufficient for building applications. Moreover, we demonstrate the unprecedented recyclability and sustainability of our transpiring wood.

# Experimental

### Fabrication of transpiring wood

Norway spruce (*Picea abies*) wood tangential sections were cut with a circular saw. A commercial 10.6 μm $CO_2$ laser engraver (Speedy 300, Trotec) was used to produce the laser-drilled wood with the desired pattern. The power of the laser beam is 20 W, the scan rate is 2.5 mm $s^{-1}$, and the image density is 1000 pulses per inch. The defocus distance is zero. The diameter of laser-drilled pattern is approximately 200 μm on the top surface. Afterward, the laser wood samples were immersed in a 0.01 M NaOH aqueous solution (Sigma-Aldrich) for 24 hours at room temperature. In a subsequent step, the NaOH-pretreated wood samples were impregnated in a 30% w/v $CaCl_2$ aqueous solution (anhydrous, powder, 99.99%, Sigma-Aldrich) for 24 hours at room temperature under gentle stirring. The composite was then dried at 103 °C for 24 hours.

### Material characterization

The morphology and element composition of the samples was characterized by a scanning electron microscope (SEM; FEI Quanta 200F, Hillsboro, OR, USA) equipped with energy dispersive X-ray spectroscopy (EDXS; Ametek-EDAX). A Pt–Pd (80/20) coating of ~10 nm thickness was applied to the samples with a sputter coater (CCU-010, Safematic, Switzerland). The Fourier transform-infrared spectra were acquired on a Bruker FT-IR equipped with an attenuated total reflectance (ATR) module. Thermogravimetric analysis were performed using a Q50 TGA (TA instruments) with a heating rate of 10 °C $min^{-1}$ in a $N_2$ atmosphere (60 mL $min^{-1}$ sample purge flow, 40 mL $min^{-1}$ balance purge flow in the 30–1000 °C temperature range), on ~10 mg of wood specimens. X-ray microtomography was performed with an EasyTom XL Ultra 230–160 device (RX Solutions, France) at an acceleration voltage of 95 kV. Images were collected with a flat panel detector. Tensile tests were performed using a universal testing machine (Zwick Roell) equipped with a 10 kN load cell. Ten specimens of each sample with the dimensions 5 × 50 × 1.5 $mm^3$ (tangential × longitudinal × radial) were tested in longitudinal direction with a span length of 25 mm. The testing speed was 0.5 mm $min^{-1}$. The displacement was measured with a travel sensor on the machine. The tensile tests were conducted at 20 °C and 65% relative humidity.

### Moisture stability

The moisture stability was measured with a leaching test by exposing freshly prepared transpiring wood samples to different conditions (95% R.H., fog, immersion in liquid water) for 24 hours. The weight change was calculated after the leaching test. For testing the dimensional stability, transpiring wood specimens were oven-dried at 103 °C for 24 hours. The specimen size on tangential, radial, and longitudinal direction were recorded as $\alpha_{t,dry}$, $\alpha_{r,dry}$, $\alpha_{l,dry}$, respectively. The specimens were then conditioned at 23 °C at a relative humidity (R.H.) of 95% for 24 hours. The specimen size on tangential, radial, and longitudinal direction were recorded as $\alpha_{t,wet}$, $\alpha_{r,wet}$, $\alpha_{l,wet}$, respectively. The swelling ratio was calculated with eqn (1)–(3):

$$\text{Swelling ratio}_{\text{tangential direction}} = (\alpha_{t,wet} - \alpha_{t,dry})/\alpha_{t,dry} \quad (1)$$

$$\text{Swelling ratio}_{\text{radial direction}} = (\alpha_{r,wet} - \alpha_{r,dry})/\alpha_{r,dry} \quad (2)$$

$$\text{Swelling ratio}_{\text{longitudinal direction}} = (\alpha_{l,wet} - \alpha_{l,dry})/\alpha_{l,dry} \quad (3)$$

### Water vapor sorption isotherms

Dynamic water vapor adsorption and desorption was measured by an automated sorption balance device (DVS Advantage ET85, Surface Measurement Systems Ltd). Ten milligrams of each sample were first dried for 10 h at 60 °C and at a partial water vapor pressure of $p/p_0 = 0$. The samples were then exposed to ascending $p/p_0$ steps of 0, 0.05, 0.10, 0.15, 0.20, 0.25, 0.30, 0.40, 0.60, 0.80, 0.85, 0.90, 0.95, and 0.98 for adsorption and then descending in the same manner for desorption at 25 °C. Equilibrium in each step was defined to be reached at a mass change per time ($dm/dt$) of less than 0.0005% $min^{-1}$ over a 10 min window or a maximal time of 1000 min per step. The samples were exposed to a flow rate of 200 sccm, and the carrier gas used was $N_2$.

### Water vapor sorption cyclic test

In order to measure the water vapor sorption performance of transpiring wood in a time-wise manner, we carried out

 

10 cycles of measurements. The transpiring wood sample was first dried for 10 h at 60 °C. Two treatment steps were then performed: $p/p_0$ 0.98 at 20 °C, $p/p_0$ = 0 at 40 °C. Equilibrium in each step was defined to be reached at a mass changer per time ($dm/dt$) of less than 0.001% over a 10 min window or a maximum time of 720 min per step.

### Moisture buffer value measurement

The humidity regulation behavior of transpiring wood was studied by measuring the moisture buffer value (MBV) according to the NORDTEST method.[14,15] A dedicated experimental set-up was designed, in which specimens of each material were introduced in a climatic chamber. The specimen dimension was 150 mm × 150 mm × 3 mm (width × height × thickness). Each specimen was sealed on five out of six sides using aluminum film to ensure vapor exchange only occur through a single face of the specimen. The specimen was pre-conditioned at 23 °C at a R.H. of 50%. The specimen was exposed to a daily cyclic variation of ambient humidity (8 h at 75% R.H. and 16 h at 33% R.H.) in the climate chamber. The moisture buffer value was then calculated from moisture uptake and release with the eqn (4):

$$\mathrm{MBV} = \Delta m/(A(\mathrm{RH}_{\mathrm{high}} - \mathrm{RH}_{\mathrm{low}})) \quad (4)$$

where MBV is the moisture buffer value (g m$^{-2}$ RH$^{-1}$), $\Delta m$ is the moisture uptake/release during the period (g) measured with a balance, $A$ is the open surface area ($m^2$), $\mathrm{RH}_{\mathrm{high/low}}$ is the high/low R.H. level (%). For each material, the MBV was the average value of the seven tested specimens. Temperature and R.H. were measured continuously with sensors in the climatic chamber; the air velocity in the surroundings of the specimens ranged from 0.1 to 0.4 m s$^{-1}$ for horizontal velocity and was lower than 0.15 m s$^{-1}$ for vertical velocity.

### Latent heat of desorption

The latent heat of water desorption in different samples was determined by differential scanning calorimetry (DSC Q2000 TA instruments). All samples were stabilized in 95% R.H. at 20 °C and allowed to reach an equilibrium moisture content state before measurement. Approximately 10 mg samples were placed into a Tzero® aluminium pan. The samples first equilibrated at 20 °C and the analysis was performed in the isothermal mode for 720 min.

### Climate regulation test

The setup for climate regulation tests was composed of three units: (1) house model (the test house framework is made of plastic board with four openings, or ''windows'', to mount the samples). The non-hygroscopic reference samples (poly(methyl methacrylate) panels), as well as the hygroscopic materials (native wood, transpiring wood with different thicknesses) are mounted in the ''windows''. (2) Climate chamber (controls the ambient temperature and humidity values, monitored by sensors). (3) Sensors and recording (indoor temperature and humidity were monitored with sensors installed in the middle indoor space. Four thermocouple sensors were installed on the surface of the samples to monitor the surface temperature. Data were recorded by the data logger. The house model was placed in the climate chamber, where ambient temperature and humidity can be well-controlled. When subjecting to different ambient climates, the changes in indoor climate and sample surface temperature were recorded by the sensing unit.

Test conditions: dynamic humidity condition was set to simulate the diurnal humidity change, that is humid nighttime and dry daytime. The ambient climate was controlled as: night time: 23 °C, 75% R.H., 8 hours; day time: 23 °C, 30% R.H., 16 hours. For roughly calculating the energy-saving potential of transpiring wood for different climate types, five testing conditions representative for characteristic climate types were tested. (i) Night time: 10 °C, 70% R.H., 12 hours; day time: 15 °C, 50% R.H., 12 hours. (ii) Night time: 15 °C, 90% R.H., 12 hours; day time: 25 °C, 50% R.H., 12 hours. (iii) Night time: 15 °C, 90% R.H., 12 hours; day time: 30 °C, 40% R.H., 12 hours. (iv) Night time: 20 °C, 90% R.H., 12 hours; day time: 40 °C, 30% R.H., 12 hours. (v) Night time: 25 °C, 70% R.H., 12 hours; day time: 35 °C, 40% R.H., 12 hours.

### Life cycle assessment

The LCA analysis was conducted using OpenLCA 1.11.0 and assessed by Environmental Footprint (Mid-point indicator) impact method. The environmental impacts of each production process were assessed by the functional unit of 'one kg of transpiring wood', including the production of raw materials, consumption of electricity, and waste disposal. The production systems, system boundaries, and life cycle inventory are detailed in the ESI.†

## Results and discussion

### Transpiring wood fabrication

**Native wood.** Wood has a characteristic hierarchical structure, featuring a predominant fiber direction (Fig. 1a). The hollow cell structure ensures efficient water transport in the longitudinal direction, while the dense cell wall (mainly composed of the biomacromolecules cellulose, hemicellulose, and lignin) copes with the load-bearing function but also makes moisture transport perpendicular to the fiber direction slower than in fiber direction (Fig. 1b–d). The naturally limited moisture adsorption capacity and the slow moisture exchange rate are critical factors restricting the application of native wood as a passive climate-regulating material. Here we address these challenges by a two-step process.

**Lasered wood.** First, we used a laser engraver to drill pore arrays in the tangential plane of spruce wood (Fig. 1e). The laser-drilled channels have a diameter of around 200 μm (Fig. 1f and Fig. S2, Movie S1, ESI†). The wood fibers were cut open, and moisture can directly propagate *via* the laser-drilled channels instead of having to penetrate through the dense cell walls (Fig. 1g). This resulted in a strong increase in the moisture exchange rate (Fig. 1h). Because of the laser-drilled pores, the tensile strength decreased from ~70 MPa to ~30 MPa, and the density from ~450 kg m$^{-3}$ to ~390 kg m$^{-3}$ due to wood ablation (Fig. S3 and Tables S1, S2, ESI†).

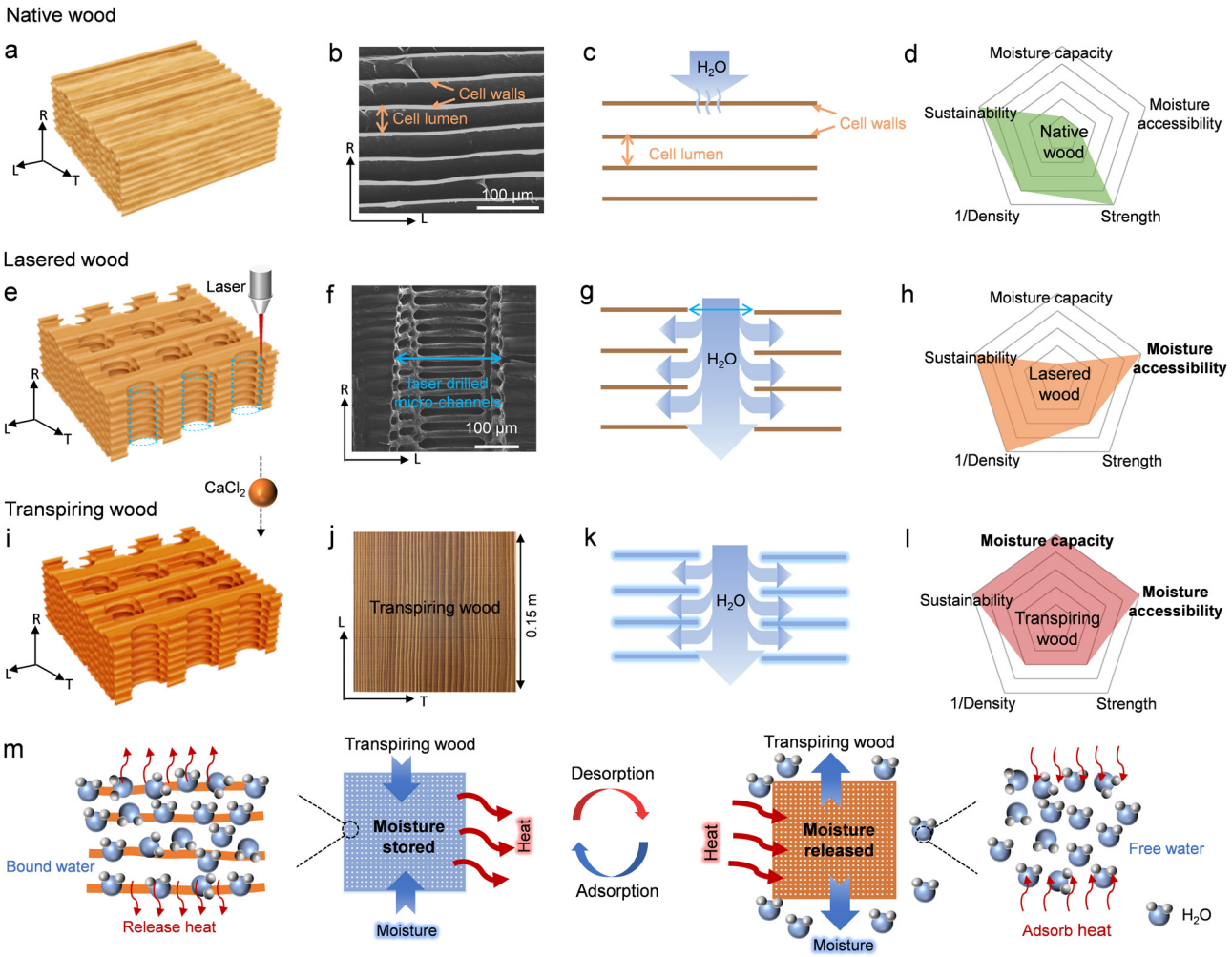


Fig. 1 Manufacturing process and working mechanism of transpiring wood. Structure and properties of (a–d) native wood, (e–h) lasered wood, and (i–l) transpiring wood (r × l × t represents radial × longitudinal × tangential directions). (a) Illustration showing the native wood structure. (b) Scanning electron microscopy (SEM) image of a native wood sample in the RL plane. (c) An illustration of the relatively low moisture exchange perpendicular to fiber direction in native wood because of the cell walls. (e) An illustration of the laser drilling process of wood. (f) SEM image of the lasered wood in the RL plane showing that the wood fibers are cut open. (g) An illustration showing the improved moisture accessibility in lasered wood thanks to the opening of pores in the cell wall. (i) A schematic image of the top-down approach used to turn lasered wood into transpiring wood by impregnation with $CaCl_2$ aqueous solution at ambient temperature and pressure. (j) Photograph of a transpiring wood sample. (k) An illustration showing the improved moisture capacity of transpiring wood thanks to the introduction of highly hygroscopic $CaCl_2$. (d, h and l) Radar plots showing the performance of (d) native wood, (h) lasered wood, and (l) transpiring wood. (m) Schematic representation of moisture adsorption and desorption by transpiring wood. During moisture adsorption the binding of water molecules releases heat due to the phase change from vapor to bound water, leading to a temperature rise. By contrast, during moisture desorption (an endothermic process) water molecules are released into the environment in the vapor state, resulting in a temperature decrease.

**Transpiring wood.** Second, we further improved the moisture adsorption capacity by a simple chemical modification. The lasered wood was pretreated with a sodium hydroxide NaOH solution (Fig. S4, ESI†). The NaOH pretreatment exchanges the protons from wood carboxylic acid groups with sodium cations (as shown by the disappearance of the characteristic –COOH peak from the infrared spectrum, Fig. S5a and b, ESI†), facilitating the successive impregnation step.[16] The NaOH-pretreated lasered wood was then impregnated with a $CaCl_2$ aqueous solution (Fig. 1i). During impregnation, some of the $Ca^{2+}$ cations were adsorbed by the cell wall through cation exchange with surface $–COO^-$ groups. When the cation exchange occurs, two $Na^+$ cations are displaced by a single $Ca^{2+}$, forming ionic complexes such as $(–COO)_2Ca$ (Fig. S4, ESI†).[17] However, this cation exchange process makes up for only a fraction of the total $CaCl_2$. The final product is composed of ~60% of wood and ~40% $CaCl_2$ (Fig. S5c and d, ESI†). The energy dispersive X-ray spectroscopy mapping images of transpiring wood showed the uniform dispersion of $CaCl_2$ in the wood scaffold (Fig. S6, ESI†). We call this final product 'transpiring wood' (Fig. 1j). The hygroscopicity of solid $CaCl_2$ is well-known.[18] Thus, using a simple procedure we are able to transform native wood into a highly hygroscopic material with high water adsorption capacity as well as moisture exchange rate (Fig. 1k and l). After the

 

impregnation with $CaCl_2$, the density of the material increased to $\sim$650 kg m$^{-3}$ while the tensile strength remained comparable to that of lasered wood. Transpiring wood is moisture-stable, no leaching was observed after performing wet/dry cycles (up to 95% R.H.). Increasing moisture content of transpiring wood led to swelling, with different extents in the main directions, due to anisotropic structure of wood. At 95% R.H., transpiring wood showed a swelling ratio of $\sim$4.7% in the tangential direction and $\sim$2.1% in the radial direction. In the longitudinal direction, the transpiring wood showed a minimal swelling ratio ($\sim$0.18%). Native spruce wood shows a maximum swelling ratio of 8.5% in the tangential direction, 3.7% in the radial direction, and 0.2–0.4% in the longitudinal direction.[19] The transpiring wood swelled substantially less than native wood in the tangential and radial directions. However, when immersed in liquid water, the loaded $CaCl_2$ was leached out (Fig. S7 and S8, ESI†). While liquid water is undesirable for the applications scenarios in building walls, this feature is also highly beneficial as it allows the direct recovery and recycling of both wood substrate and $CaCl_2$ at the end of the product's lifecycle.

### Mechanism of the hygrothermal effect

The hygrothermal effect results from the combination of the moisture adsorption/desorption and heat release/uptake between the hygroscopic material and the environment. During moisture exchange between the hygroscopic material and the surrounding atmosphere, water undergoes a phase change. In the adsorption process, hygroscopic materials store moisture by binding water molecules. When water vapor changes into bound water, the associated energy of this phase change is released as heat to the environment. By contrast, during the desorption process, moisture is released into the environment and extra energy is needed for water to change from the liquid state to vapor. Therefore, the temperature of the material is reduced. The amount of heat exchanged in these processes is the so-called latent heat of sorption (Fig. 1m).[20,21] This effect can be utilized for improving indoor thermal comfort while reducing energy consumption. Environmental humidity varies significantly over a single day as well as during changing seasons. By adsorbing and desorbing water from the environment, hygroscopic materials have the ability to passively influence the humidity and consequently the temperature of the surrounding atmosphere. In the present work, we demonstrate that our transpiring wood with enhanced hygrothermal performance can take advantage of the coupled effects of moisture buffering (thanks to water sorption) and heating (thanks to the latent heat of sorption).

### Moisture buffering performance of transpiring wood

Hygroscopic materials can be used to balance extreme humidity levels by the reversible adsorption and desorption of water, an approach called moisture buffering.[22,23] The moisture buffering value measures the ability of porous materials to buffer changes in humidity by adsorbing and desorbing water vapor from the surrounding air. As mentioned above, the natural hygroscopicity of wood is usually considered highly detrimental for practical applications in the building sector. However, this is not the only reason why native wood has not yet been considered specifically for humidity and thermal regulation. Another reason is linked to the effective humidity range relevant for building applications.[24,25] Between 0–20% R.H., wood has a moisture content between 0–6%. The water molecules are strongly adsorbed by the cell wall and form a monomolecular layer, with the concomitant release of heat due to the phase change from water vapor to bound water. In the range of 20–70% R.H., physical adsorption results in the formation of a multilayer of water molecules, with the release of less heat. In the range of 75–100% R.H., water vapor is condensing and the water content increases to $\sim$30% for wood species like spruce (Fig. 2a). Therefore, for native wood, a useful hygrothermal effect happens only in the low humidity range (0–20% R.H.), which is not relevant for real-world building conditions. In addition, in native wood the rate of moisture exchange perpendicular to the fiber is reduced by the dense cell walls.[26,27]

Our transpiring wood addresses the above-mentioned limitations by improving moisture sorption capacity and facilitating moisture exchange. $CaCl_2$ has a water adsorption capacity of $\sim$700% and is highly hygroscopic. The transpiring wood showed a water adsorption capacity of $\sim$350%, 14 times higher compared to native wood, together with high moisture stability. After a ten-cycle measurement, the sample revealed no loss of water sorption capacity (Fig. 2b). The moisture buffer value increased from 0.78 for native wood to 13.82 for transpiring wood (18 times higher), which represents a substantial improvement especially compared to common building materials (Fig. 2c, d and Tables S3, S4, ESI†).[28]

### Thermal energy storage performance of transpiring wood

When discussing the transfer of moisture, the coupled transfer of heat needs to be taken into consideration as well. Our transpiring wood also possesses excellent thermal energy storage performance, using water as a phase change material, by adsorbing and releasing moisture from and to the environment. To prove this, we studied the latent heat of desorption by differential scanning calorimetry (DSC) (Fig. S9 and Table S5, ESI†). The latent heat of water-saturated transpiring wood is 2058 J g$^{-1}$, that is 9 times higher compared to state-of-the-art wood-phase change material composites (Fig. 2e and f).[29–33]

We investigated the surface temperature change of the transpiring wood when exposed to dynamic humidity changes (Fig. 2g), from 90% to 20% R.H., while keeping the ambient temperature at 30 °C. With native wood, a surface temperature change of 4 °C (from 30 °C to 34 °C) was measured. By contrast, the surface temperature of transpiring wood raised to 38 °C because of water adsorption and decreased to 26 °C because of water desorption, corresponding to a surface temperature change of 12 °C (three times higher than with native wood) (Fig. 2h, i and Fig. S10, ESI†). The latent heat of water phase change during adsorption/desorption contributed to the temperature change of the sample, which in turn had an impact on the surrounding space.

We further investigated the influence of wood species, studying the performance of spruce (softwood), maple (hardwood), poplar

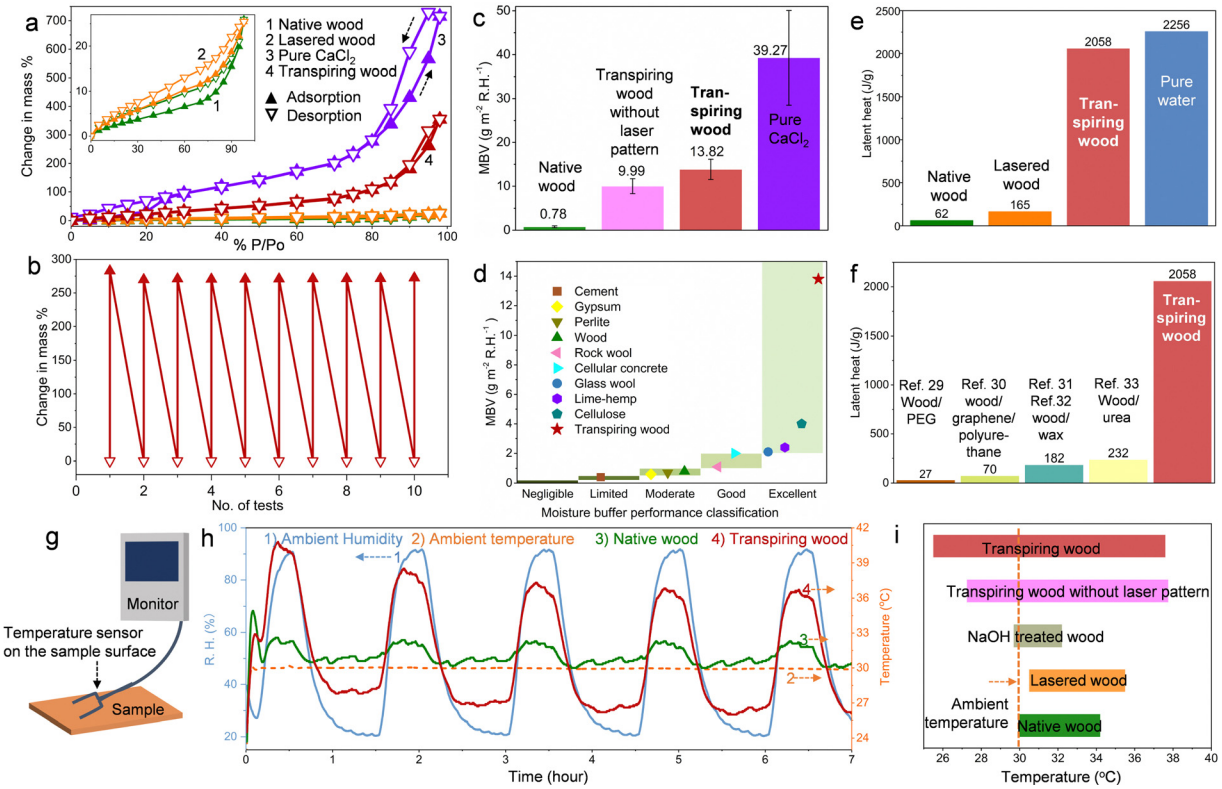


Fig. 2 Moisture sorption performance of transpiring wood at the material level. (a) Water sorption isotherms of native wood, lasered wood, $CaCl_2$ powder, and transpiring wood at 25 °C. (b) Water-uptake profile swung between 0–98% R.H. for ten cycles. (c) Moisture buffer value of native wood, wood-$CaCl_2$ composite (without lasered pores), $CaCl_2$ powder, and transpiring wood. (d) Moisture buffer performance classification of common building materials and transpiring wood. (e) Calculated latent heat of water-saturated samples from isothermal differential scanning calorimetry (DSC). (f) Comparison of the latent heat of transpiring wood with that of previously reported wood-phase change material composites. (g) An illustration showing the set-up of monitoring the materials' surface temperature during the water sorption/desorption. (h) Surface temperature changes of native and transpiring wood resulting from the exposure to dynamic humidity swings (between 20% and 90% R.H.) at 30 °C ambient temperature. (i) The range of surface temperature change of transpiring wood compared to its precursors.

(hardwood), and birch (hardwood). Samples were exposed to dynamic humidity swings (between 20% and 90% R.H.) at 30 °C ambient temperature. Surface temperature changes of different transpiring wood samples are shown in Fig. S11, ESI.† The results showed that transpiring wood based on different wood species exhibited similar hygrothermal performance. In this work, we selected spruce wood as a representative wood. Norway spruce (*Picea abies*) is highly abundant in northern and central Europe, and widely used in the construction sector.

### Climate regulation performance of transpiring wood

Subjected to dynamic humidity changes in a closed space, our transpiring wood can regulate humidity as well as temperature. We further investigated the influence of this hygrothermal effect on the surrounding environment in a model system. We built a test house model with four sample test "windows", humidity and temperature sensors, and a data recording unit. The model was placed in a climate chamber to ensure control of the external temperature and humidity (Fig. 3a and Fig. S12, ESI†). When the humidity is high, the transpiring wood takes up water and releases heat. As a consequence, humidity declines and the indoor temperature increases by the released heat. When the humidity is low, the transpiring wood releases water to the environment, taking the necessary energy from the environment. As a result, the humidity is increased while the indoor space is cooled down (Fig. 3b and c).

**Humidity regulation.** In a following round of tests, we applied conditions simulating the diurnal humidity change, that is humid nighttime and dry daytime. The ambient temperature was kept at 23 °C, while the ambient humidity was initially kept at 75% R.H. for 8 hours (adsorption stage) and then changed to 30% R.H. for another 16 hours (desorption stage) (Fig. S13 and S14, ESI†). In Fig. 3d–f, the humidity regulation effects of a non-hygroscopic material (reference material: poly(methyl methacrylate), PMMA) and hygroscopic materials (native wood, transpiring wood with different thickness) are compared. The non-hygroscopic reference material does not interact with moisture and has negligible moisture buffer capacity. When the ambient R.H. swung from 75% to 30%, the indoor humidity with reference material windows fluctuated together with the ambient humidity and led to a high range of R.H. change, from 70% to 33%. With native wood, the moderate moisture buffer capacity led to indoor R.H. fluctuations of 35–64%. For transpiring wood, the moisture buffer capacity is 18 times higher than for

 

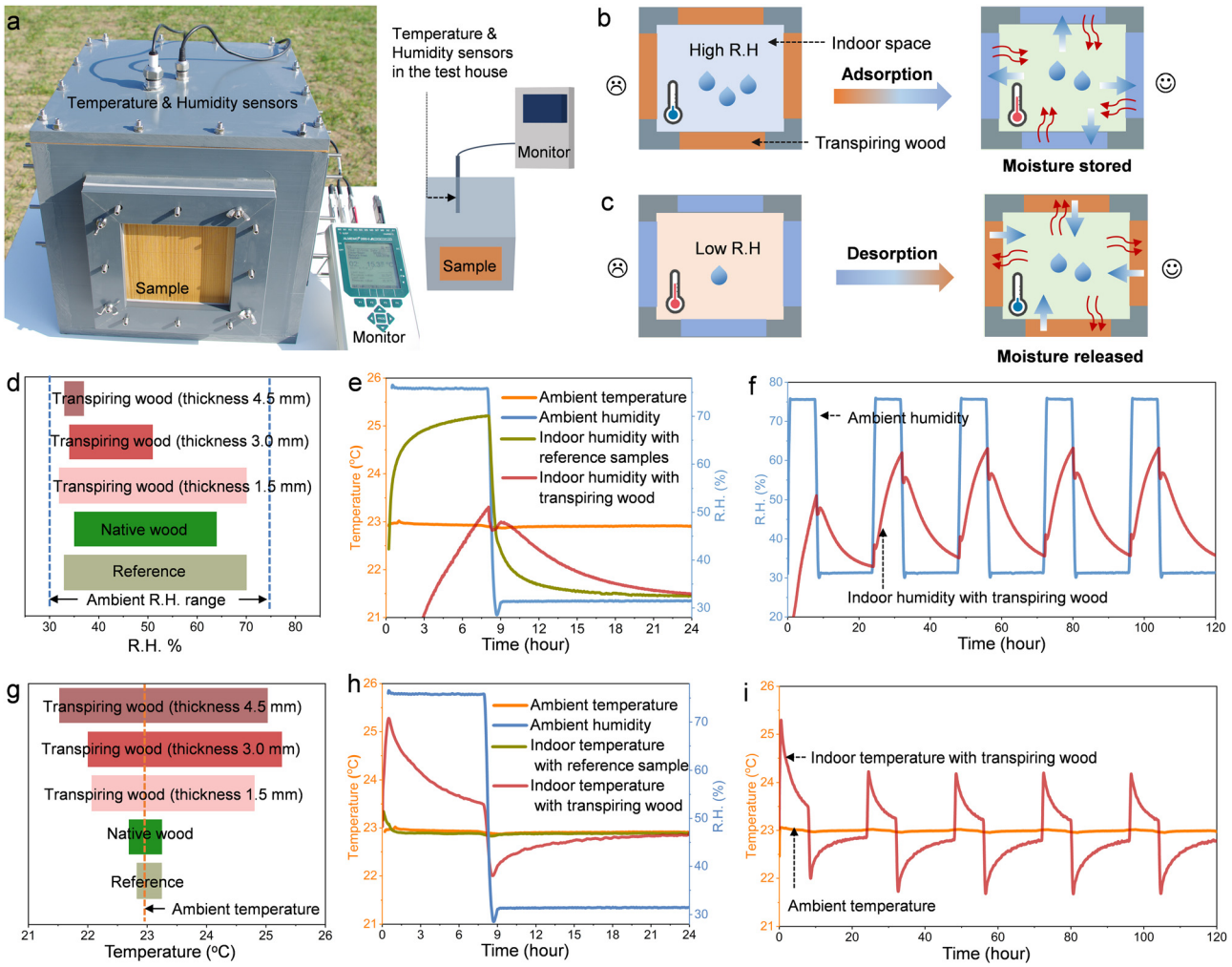


Fig. 3 Investigation of the macroscopic hygrothermal effect of transpiring wood on a system level. (a) A test house made of four transpiring wood walls and equipped with temperature and humidity sensors. (b) When moisture is adsorbed by transpiring wood, the humidity inside the test house (indoor) is decreased while the indoor temperature increases. (c) During the water desorption process moisture is released, leading to an increase in indoor humidity, while the endothermic process cools the indoor air. (d–f) Humidity regulation performance test. (d) Indoor humidity ranges resulting from the use of different wall materials. (e) Indoor humidity curves resulting from dynamic climate conditions (75% R.H. and 23 °C, 8 hours; 30% R.H. and 23 °C, 16 hours). (f) Five cycles of the humidity regulation performance test using transpiring wood. (g–i) Temperature regulation performance. (g) Indoor temperature range resulting from the use of different wall materials. (h) Indoor temperature curves resulting from dynamic climate conditions (75% R.H. and 23 °C, 8 hours; 30% R.H. and 23 °C, 16 hours). (i) Five cycles of the temperature regulation performance test using transpiring wood.

native wood. The results revealed that the thickness of the transpiring wood membrane remarkably influenced the humidity regulation performance. While the 1.5 mm membrane thickness led to minimal regulation performance (from 32–70%), 4.5 mm membrane thickness led to too low humidity (from 33–37%). Both the high humidity fluctuation and excessively dry indoor climate are not ideal. In this work, we optimized the membrane thickness of transpiring wood to 3.0 mm. During an ambient R.H. fluctuation from 75% to 30%, the transpiring wood with a thickness of 3.0 mm was able to buffer the high R.H. fluctuation and maintained the indoor R.H. between 34–51%. The humidity regulation performance of transpiring wood was able to counterbalance the humidity fluctuation in the time range of 24 hours, demonstrating great potential for buffering real-world diurnal humidity fluctuations.

**Thermal regulation.** The humidity regulation performance makes our transpiring wood an excellent passive humidity regulation material for improving indoor living comfort. Moreover, the coupled effect to latent heat during water sorption and desorption leads to thermal regulation ability, which further leads to potential energy-saving in buildings. Fig. 3g–i shows the associated thermal regulation performance. No obvious indoor temperature change was measured with the non-hygroscopic reference sample during humidity fluctuation. Native wood also did not lead to obvious indoor temperature changes because of the low moisture sorption capacity. By contrast, when exposed to 75% R.H., the transpiring wood samples adsorbed water and their surface temperature increased. This adsorption process released heat and led to a rise of the indoor temperature. The indoor temperature increased to

~25 °C (2 °C higher than ambient temperature). When the ambient climate changed to low humidity, the humid transpiring wood sample released moisture into the environment, resulting in a cooling effect. The indoor temperature was decreased to 22 °C and 1 °C lower than ambient temperature (Fig. 3g and h). Although the thickness of the transpiring wood had a remarkable influence on the humidity regulation performance, its influence on thermal regulation performance was minor.

**Cyclic stability.** We further measured the stability of both humidity and thermal regulation performance by means of cyclic tests. The ambient temperature was hold at 23 °C, and the ambient humidity changed from 73% to 30% for 5 cycles (24 hours per cycle). With the transpiring wood, the indoor R.H. was maintained between 35% and 60%, avoiding high humidity fluctuation and favoring living comfort. The indoor temperature was increased by the water adsorption of transpiring wood and reduced by the water desorption process and this performance was stable over several cycles (Fig. 3f, i and Fig. S15, ESI†). The cyclic tests demonstrated the excellent long-term humidity and thermal regulation performance of our transpiring wood.

### The energy efficiency of transpiring wood

Building energy consumption accounts for ~30% of the total energy consumption around the world, and for which heating and cooling systems are the most responsible. The energy consumption in buildings for heating and cooling is closely associated with the different climate types. Massive amounts of energy are necessary to maintain the indoor temperature against the diurnal temperature fluctuations. For example, in moderate climate countries ~13% of energy is used for heating while only ~3% of energy is used for cooling. By contrast, in cold climate countries, about 50% of the total building energy

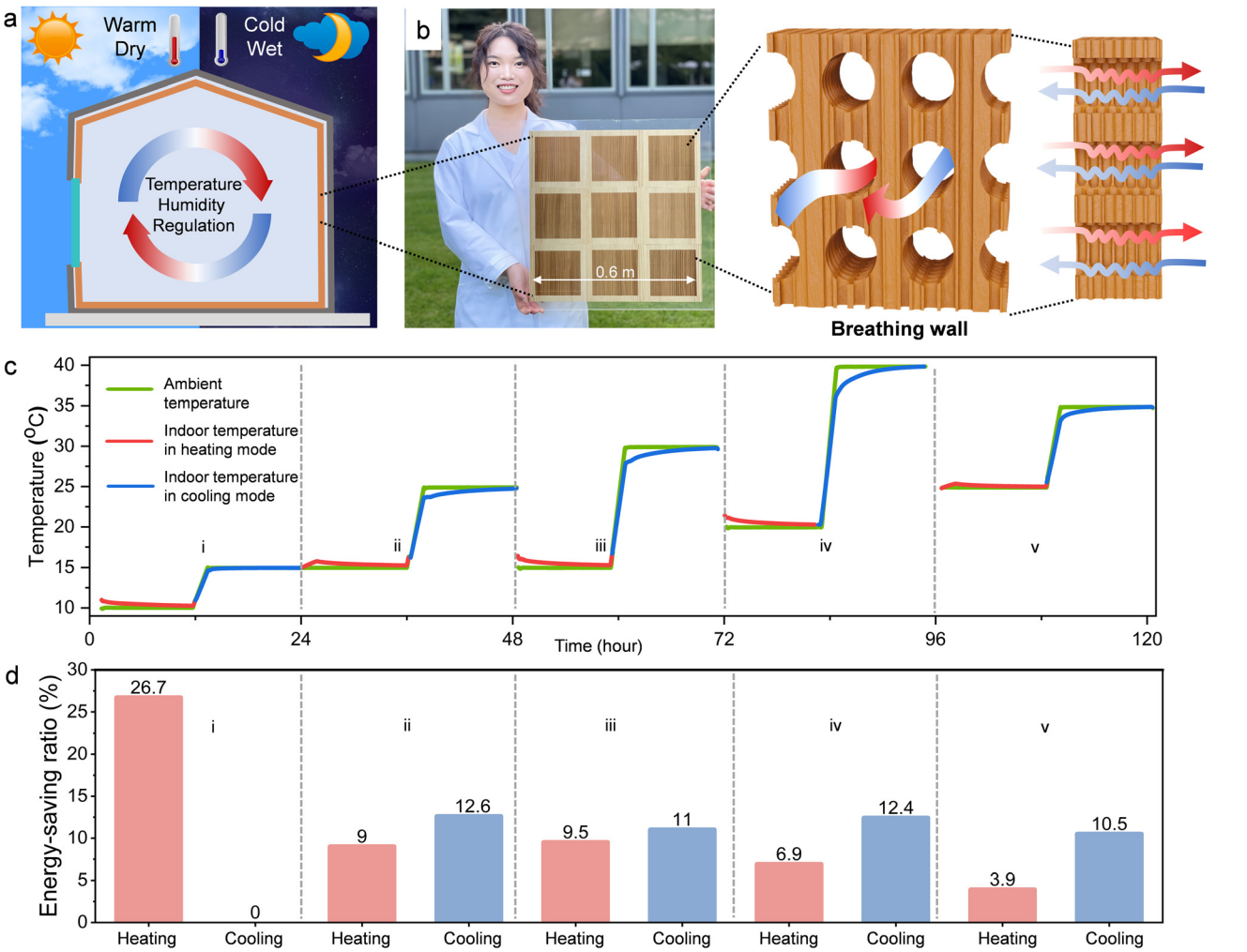


Fig. 4 Proposed applicative scenarios for transpiring wood and its positive impact on energy saving. (a) Transpiring wood could be used as breathable walls in buildings for passive indoor climate regulation. (b) A breathable wall panel demonstrator composed of nine transpiring wood modules, along with its schematic representation. (c) Thermal regulation performance of transpiring wood walls under various climate types. (i) Night time: 10 °C, 70% R.H., 12 hours; day time: 15 °C, 50% R.H., 12 hours. (ii) Night time: 15 °C, 90% R.H., 12 hours; day time: 25 °C, 50% R.H., 12 hours. (iii) Night time: 15 °C, 90% R.H., 12 hours; day time: 30 °C, 40% R.H., 12 hours. (iv) Night time: 20 °C, 90% R.H., 12 hours; day time: 40 °C, 30% R.H., 12 hours. (v) Night time: 25 °C, 70% R.H., 12 hours; day time: 35 °C, 40% R.H., 12 hours. (d) Energy-saving ratio for heating/cooling under different climate types when transpiring wood was used to reduce the indoor temperature fluctuation under various climate types.

 

consumption is used for heating and only ~5% of the energy is used for cooling. In warm climates, a major part of energy is consumed for cooling.

Thanks to the hygrothermal effect, we envisage an application of our transpiring wood as interior walls in non-climate-sealed buildings (Fig. 4a). Fig. 4b shows the demonstrator of a breathable wall panel composed of nine transpiring wood modules. The thermal regulation performance of the transpiring wood suggests its potential in reducing energy consumption of buildings for space heating and cooling.[34] We envisage that transpiring wood is able to heat up the indoor air by water adsorption during the humid and cool night time, while cooling down the indoor air by water desorption during the dry and warm day time. This buffering effect could lower the peaks and valleys during diurnal temperature fluctuations and thus lead to indirect energy saving for maintaining indoor temperature.

To study the potential of transpiring wood for energy-savings, we tested the thermal regulation performance of transpiring wood with five characteristic climate types, respectively: (i) night time: 10 °C, 70% R.H., 12 hours; day time: 15 °C, 50% R.H., 12 hours. (ii) Night time: 15 °C, 90% R.H., 12 hours; day time: 25 °C, 50% R.H., 12 hours. (iii) Night time: 15 °C, 90% R.H., 12 hours; day time: 30 °C, 40% R.H., 12 hours. (iv) Night time: 20 °C, 90% R.H., 12 hours; day time: 40 °C, 30% R.H., 12 hours. (v) Night time: 25 °C, 70% R.H., 12 hours; day time: 35 °C, 40% R.H., 12 hours. The transpiring wooden walls decreases the indoor temperature fluctuation. Therefore, less energy needs to be consumed to maintain the ideal indoor temperature (Fig. 4c, d and Fig. S16, ESI†). Our rough calculations show that in cold climates (climate type i), the energy for heating is decreased by 26.7% with no observable difference for cooling. In mild climates (climate type ii and iii), the use of transpiring wood results in ~9% energy saving for heating and ~12% for cooling. In warm climates (climate type iv and v), the cooling effect is even more prominent. The use of transpiring wood allowed saving between 4–7% heating energy and 10–12% cooling energy. According to the results of our experimental climate tests, the transpiring wood contributes better to heating in cold climate and works better in cooling mode under warm climate. In mild climates, the transpiring wood showed a balanced performance in both heating and cooling mode. Moreover, our transpiring wood is able to maintain the indoor humidity in the comfortable level in all climate types (Fig. S17, ESI†). These findings have great practical relevance in terms of energy savings.

It is noteworthy that these calculations are based on the assumption that the indoor temperature and humidity fluctuate in tandem with the ambient climate when the climate regulation effects of transpiring wood are activated. Therefore, these energy-saving efficiencies can only be achieved when the

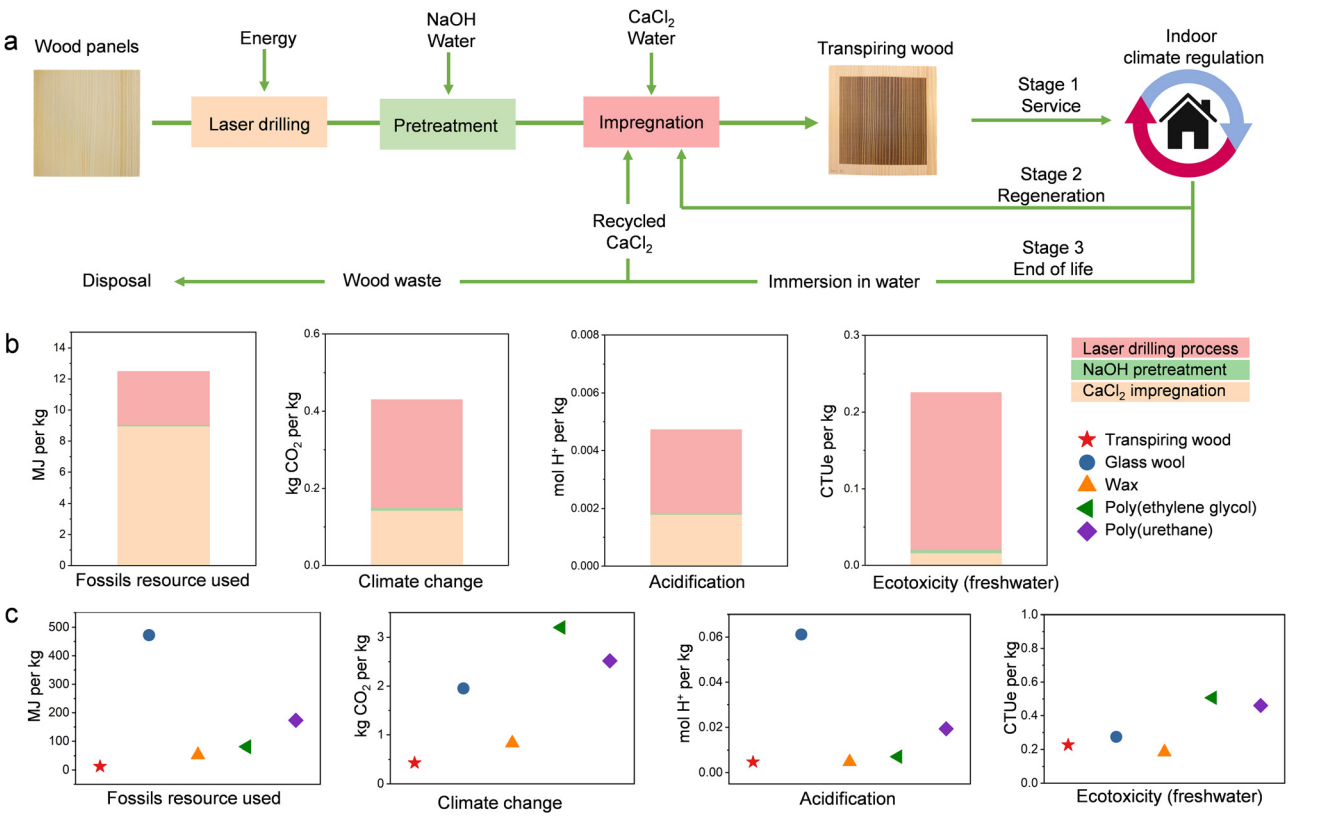


Fig. 5 The environmental impact of transpiring wood. (a) An illustration of the production system and recyclability of transpiring wood. (b) The environmental impact for each production step of transpiring wood. CTUe is the comparative toxicity unit for ecotoxicity. (c) Environmental impact indicators of transpiring wood compared to those of glass wool, wax, poly(ethylene glycol), and poly(urethane).

transpiring wood does not work collaboratively with an HVAC system. While preventing its use in conventional climate-sealed buildings, this makes its use especially favorable in large, energy-intensive industrial production facilities or in farm buildings, which often lack proper thermal insulation.

### The environmental impact of transpiring wood

The fabrication process of transpiring wood meets sustainability criteria (Fig. 5a). There are two main aspects to be considered in terms of sustainability: the source of materials and the fabrication process. Compared to bottom-up strategies, our top-down fabrication process is energy- and time-efficient. Already with one-step of laser drilling, a remarkable increase in the moisture exchange rate could be achieved. The subsequent pretreatment and chemical impregnation required no vacuum, organic solvents or heating, water and ambient conditions being sufficient. The only resources consumed are wood and $CaCl_2$, renewable and abundant, respectively.

Transpiring wood, used to make or decorate the interior walls of a building, can help to maintain a comfortable indoor climate and even to decrease the energy consumption of buildings for the regulation of indoor humidity and temperature. During its service life, if necessary the transpiring wood can be refreshed by immersion in a 30 wt% $CaCl_2$ solution. At the end of the product life, the $CaCl_2$ can be removed from the transpiring wood simply by immersion in water and the resulting solution can then be recycled. Overall, transpiring wood showed sustainability, moisture capacity, and moisture exchange rate highly superior to conventional materials used for thermal and/or humidity regulation, together with a satisfying mechanical performance.

To better quantify the environmental impact of the transpiring wood, we conducted a simple cradle-to-gate life cycle assessment.[35,36] The environmental impact indicators are (i) fossil resources used, (ii) climate change, (iii) acidification and (iv) ecotoxicity. Fig. 5b shows the contribution analysis for each production step. The results indicate that the laser drilling process and $CaCl_2$ impregnation step are the main contributors to environmental impacts, while the NaOH pretreatment has a minimal environmental impact in every category (Table S6, ESI†). We compared the environmental impacts of transpiring wood with those of common insulation materials such as glass wool, and of common phase change materials such as wax, poly(ethylene glycol) PEG and poly(urethane) PU (Fig. 5c and Table S7, ESI†). Across all the impact categories, the transpiring wood showed the lowest environmental impacts among the compared insulation materials and phase change materials, except for ecotoxicity, where transpiring wood has slightly higher impact than wax. The $CO_2$ footprint (global warming indicator) of transpiring wood is 0.43 kg $CO_2$ per kg, 87% less compared to PEG, a state-of-art phase-change material. It is noteworthy that the life cycle assessment input for transpiring wood was taken from laboratory-scale values, meaning that our analysis shows the environmental benefits of our material compared with fully optimized industrialized products. We assume that the production process of transpiring wood would be more energy-efficient and environmental-friendly once optimized for industrial production.

## Conclusions

We developed a transpiring wood with improved moisture uptake capacity and moisture exchange speed, suitable for the passive regulation of indoor humidity and temperature through the exchange of moisture with the environment. We proved that the hygrothermal performance of transpiring wood is effective for a variety of climates, which favors its broad application in the built environment. By decreasing the temperature fluctuation, the potential indirect energy savings are in the order of 10% for cooling and 4–27% for heating, resulting in a substantial contribution to energy savings in buildings. The use of convenient and renewable resources, together with a green fabrication process (laser drilling of wood and impregnation with $CaCl_2$), open the avenue to produce energy-efficient building material with sustainability, moisture capacity, moisture exchange rate, and mechanical performance.

## Author contributions

I. B. proposed the project. Y. D., T. K., G. P. and I. B. conceived the idea. T. K., G. P. and I. B. supervised the project. Y. D. designed the experiments. Y. D., C. D., R. Z., K. T., and S. S. carried out the experiments and analyzed the data. Y. D., I. B. and G. P. organized and wrote the manuscript. All authors contributed to the discussion and commented on the manuscript.

## Conflicts of interest

The authors declare no competing interests.

## Acknowledgements

The project was conducted in the framework of the SNF project ''Hierarchical cellulose scaffolds for structural and functional gradient materials'' (200021_184821/1). We thank the Scientific Center for Optical and Electron Microscopy at ETH Zurich for providing access to their facilities and Thomas Schnider for the wood sample preparation. Y. D. would like to thank Tongtong Wang for her help with the wall panel demonstrator.

## References

1 IEA, United Nations Environment Programme, 2021.
2 W. Wei and H. M. Skye, *Renewable Sustainable Energy Rev.*, 2021, **142**, 22.
3 A. Mastrucci, B. van Ruijven, E. Byers, M. Poblete-Cazenave and S. Pachauri, *Clim. Change*, 2021, **168**, 26.
4 M. González-Torres, L. Pérez-Lombard, J. F. Coronel, I. R. Maestre and D. Yan, *Energy Rep.*, 2022, **8**, 626–637.
5 Y. Zhang, L. Wu, X. Wang, J. Yu and B. Ding, *Nat. Commun.*, 2020, **11**, 1–11.

 

6 P. Hou, K. Zu, M. Qin and S. Cui, *Build. Environ.*, 2021, **187**, 107396.
7 J. Liang, X. Zhang and J. Ji, *J. Energy Storage*, 2021, **36**, 102395.
8 N. X. Zhu, Z. W. Wei, C. X. Chen, X. H. Xiong, Y. Y. Xiong, Z. Zeng, W. Wang, J. J. Jiang, Y. N. Fan and C. Y. Su, *Angew. Chem., Int. Ed.*, 2022, **61**, DOI: 10.1002/anie.202112097.
9 T. Li, Y. Zhai, S. He, W. Gan, Z. Wei, M. Heidarinejad, D. Dalgo, R. Mi, X. Zhao and J. Song, *Science*, 2019, **364**, 760–763.
10 R. H. Guo, L. B. Shan, Y. H. Wu, Y. M. Cai, R. Huang, H. Ma, K. C. Tang and K. Liu, *Mater. Today Energy*, 2022, **23**, DOI: 10.1016/j.mtener.2021.100888.
11 P. Wei, C. E. Cipriani and E. B. Pentzer, *Matter-Us*, 2021, **4**, 1975–1989.
12 C. Chen, Y. Kuang, S. Zhu, I. Burgert, T. Keplinger, A. Gong, T. Li, L. Berglund, S. J. Eichhorn and L. Hu, *Nat. Rev. Mater.*, 2020, **5**, 642–666.
13 C. Wang and C. Piao, *Wood Fiber Sci.*, 2011, **43**, 41–56.
14 C. Rode, R. H. Peuhkuri, K. K. Hansen, B. Time, K. Svennberg, J. Arfvidsson and T. Ojanen, *NORDTEST project on moisture buffer value of materials, AIVC Conference 'Energy performance regulation': Ventilation in relation to the energy performance of buildings*, 2005.
15 C. Rode, R. Peuhkuri, B. Time, K. Svennberg, T. Ojanen and P. Mukhopadhyaya, *Moisture buffer value of building materials*, ASTM International, 2007.
16 K. Tu, B. Puértolas, M. Adobes-Vidal, Y. Wang, J. Sun, J. Traber, I. Burgert, J. Pérez-Ramírez and T. Keplinger, *Adv. Sci.*, 2020, **7**, 1902897.
17 H. Ye, Z. Yuan, S. M. Li and L. Zhang, *Appl. Therm. Eng.*, 2014, **62**, 690–696.
18 S. Bouzenada, A. N. Kaabi, L. Frainkin, T. Salmon and A. Leonard, 7th International Conference on Ambient Systems, Networks and Technologies, 2016, **vol. 83**, pp. 718–725.
19 P. Niemz and W. Sonderegger, *Holzphysik*, Carl Hanser Verlag, 1993.
20 D. Kraniotis and K. Nore, *Procedia Environ. Sci.*, 2017, **38**, 364–371.
21 X. Zhou, G. Desmarais, S. Carl, D. Mannes, D. Derome and J. Carmeliet, *Build Environ.*, 2022, **214**, 108845.
22 C. Rode, R. H. Peuhkuri, L. H. Mortensen, K. K. Hansen, B. Time, A. Gustavsen, T. Ojanen, J. Ahonen, K. Svennberg and J. Arfvidsson, *Moisture buffering of building materials*, Technical University of Denmark, Department of Civil Engineering, 2005.
23 V. Cascione, D. Maskell, A. Shea and P. Walker, *Constr. Build. Mater.*, 2019, **200**, 333–343.
24 B. Time, *Holz Roh-Werkst.*, 2002, **60**, 405–410.
25 E. T. Engelund, L. G. Thygesen, S. Svensson and C. A. Hill, *Wood Sci. Technol.*, 2013, **47**, 141–161.
26 E. E. Thybring, S. V. Glass and S. L. Zelinka, *Forests*, 2019, **10**, 704.
27 W. Willems, *Wood Sci. Technol.*, 2017, **51**, 751–770.
28 C. Rode, R. Peuhkuri, B. Time, K. Svennberg, T. Ojanen and P. Mukhopadhyaya, *Moisture buffer value of building materials*, ASTM International, 2007.
29 A. Dorigato, G. Fredi and A. Pegoretti, *Frontiers in Materials*, 2019, **6**, 76.
30 X. Lin, S. Jia, J. Liu, X. Li, X. Guo and W. Sun, *J. Mater. Sci.*, 2021, **56**, 16570–16581.
31 S. Liu, H. Wu, Y. Du, X. Lu and J. Qu, *Sol. Energy Mater. Sol. Cells*, 2021, **230**, 111187.
32 X. Pan, N. Zhang, Y. Yuan, X. Shao, W. Zhong and L. Yang, *Sol. Energy*, 2021, **230**, 269–277.
33 N. Feng, Z. Kang and D. Hu, *Sol. Energy*, 2021, **223**, 19–32.
34 B. Duraković, *PCM-Based Building Envelope Systems: Innovative Energy Solutions for Passive Design*, Springer Nature, 2020.
35 Q. Q. Xia, C. J. Chen, Y. G. Yao, J. G. Li, S. M. He, Y. B. Zhou, T. Li, X. J. Pan, Y. Yao and L. B. Hu, *Nat. Sustain.*, 2021, **4**, 627–635.
36 I. Z. Bribian, A. V. Capilla and A. A. Uson, *Build. Environ.*, 2011, **46**, 1133–1140.